Spontaneous symmetry breaking of solitons trapped in a double-channel potential

M. Matuszewski,[1] B. A. Malomed,[2] and M. Trippenbach[1,3]

[1]*Institute of Theoretical Physics, Physics Department, Warsaw University, Hoża 69, PL-00-681 Warsaw, Poland*
[2]*Department of Interdisciplinary Sciences, School of Electrical Engineering, Faculty of Engineering, Tel Aviv University,
Tel Aviv 69978, Israel*
[3]*Soltan Institute for Nuclear Studies, Hoża 69, PL-00-681 Warsaw, Poland*
(Received 9 October 2006; published 21 June 2007)

We consider a two-dimensional (2D) nonlinear Schrödinger equation with self-focusing nonlinearity and a quasi-1D double-channel potential, i.e., a straightforward 2D extension of the well-known double-well potential. The model may be realized in terms of nonlinear optics and Bose-Einstein condensates. The variational approximation (VA) predicts a bifurcation breaking the symmetry of 2D solitons trapped in the double channel, the bifurcation being of the subcritical type. The predictions of the VA are confirmed by numerical simulations. The work presents an original example of the spontaneous symmetry breaking of 2D solitons in dual-core systems.

I. INTRODUCTION

The creation of Bose-Einstein condensates (BECs) in vapors of alkali metals has opened up a unique opportunity to investigate nonlinear interactions of atomic matter waves. In particular, an important physical problem is to develop methods allowing one to create and control matter-wave solitons in the experiment. One-dimensional (1D) dark [1], bright [2], and gap-mode [3] solitons have already been created.

Another fascinating phenomenon, viz., the Josephson effect in BEC, was observed in condensates loaded in a double-well potential. Tunneling through a potential barrier usually occurs in quantum systems on a nanoscopic scale, while the Josephson effect features the tunneling of macroscopic wave functions describing intrinsically coherent states [4]. This phenomenon has been observed in sundry systems, such as a pair of superconductors separated by a thin insulator (the Josephson effect proper) [5], and two reservoirs of superfluid helium connected by nanoscopic apertures [6,7]. Recently, a successful implementation of a bosonic Josephson junction formed by two weakly coupled BECs in a macroscopic double-well potential was reported [8]. In contrast to hitherto realized Josephson systems in superconductors and superfluids, interactions between tunneling particles plays a crucial role in the junction implemented in the BEC setting, the effective nonlinearity induced by the interactions giving rise to new dynamical regimes in the tunneling. In particular, anharmonic Josephson oscillations were predicted [9–11], provided that the initial population imbalance in the two potential wells falls below a critical value. The dynamics change drastically for the initial population difference exceeding the threshold of the macroscopic quantum self-trapping and thus inhibiting large-amplitude Josephson oscillations [12–14]. These two different regimes have been experimentally demonstrated in the BEC-based Josephson-junction arrays [15–17].

These dynamics can be well explained by means of a simple model derived from the Gross-Pitaevskii equation (GPE). Two equations for the self-interacting BEC amplitudes, linearly coupled by tunneling terms, describe the dynamics in terms of the inter-well phase difference and population imbalance. As mentioned above, the nonlinearity

specific to BEC gives rise to the "macroscopic quantum self-trapping" effect, in the form of a self-maintained population imbalance [13,18–20]. In order to derive a reduced two-state model, one needs to find eigenstates of the corresponding GPE and perform stability analysis for them. Such analysis can be readily performed for the square-shaped double-well potential, where analytic solutions are available [19–21]. In this case, the point of the symmetry-breaking bifurcation, where asymmetric solutions emerge, can be found exactly.

The present paper addresses the symmetry-breaking bifurcation and the existence and stability of asymmetric states in a two-dimensional system, which is a direct extension of the familiar double-well model [13,14]. The corresponding potential is shown in Fig. 1 below. It features the double-square-well shape in the x direction, being uniform along y. To our knowledge, the spontaneous symmetry breaking (SSB) has never been studied in 2D systems before. By means of the variational approximation (VA), we will find regions where stable asymmetric solitons exist, and the prediction will be then confirmed by direct simulations.

The paper is organized as follows. The model is introduced in Sec. II, where its physical interpretations are outlined too, in terms of BEC and nonlinear optics. Then, in Sec. III, we derive variational equations and analyze their solutions, which predict the SSB of a subcritical type. At the end of that section, we compare the result with those for the cw (continuous-wave, i.e., as a matter of fact, one-dimensional) states, for which the SSB bifurcation is of a
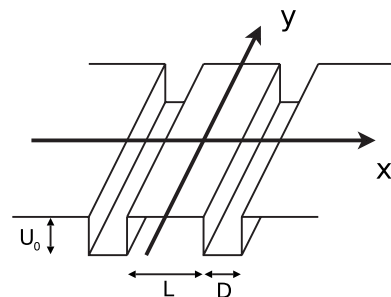

FIG. 1. The shape of the quasi-one-dimensional double-well potential $U(x, y)$.

different type, being supercritical. In Sec. IV, we compare predictions of the VA with numerical results, and Sec. V concludes the paper.

II. THE MODEL

The starting point is the 2D equation in a normalized form, with the self-attracting cubic nonlinearity

$$i\Psi_t + \frac{1}{2}(\Psi_{xx} + \Psi_{yy}) - U(x)\Psi + |\Psi|^2\Psi = 0, \qquad (1)$$

where the quasi-1D double-well potential is taken as

$$U(x) = \begin{cases} 0, & |x| < \frac{1}{2}L \text{ and } |x| > \frac{1}{2}L + D, \\ -U_0, & \frac{1}{2}L < |x| < \frac{1}{2}L + D, \end{cases} \qquad (2)$$

with D, U_0, and L being, respectively, the width and depth of each well, and the width of the barrier between them, see Fig. 1.

Equation (1) admits three different physical interpretations. In terms of BEC, it is the Gross-Pitaevskii equation, for a pancake-shaped (nearly flat) self-attractive condensate (in fact, this implies ^{7}Li, in which the scattering length can be readily made slightly negative by means of the Feshbach resonance [2]), with potential (2) acting in the (x,y) plane. In nonlinear optics, the evolutional variable, t, is actually the propagation distance (usually denoted by z). Then, one possible interpretation is that Eq. (1) is the nonlinear Schrödinger equation (NLSE) which, adopting the ordinary paraxial approximation for the diffraction, governs the stationary transmission of an optical signal in the spatial domain (i.e., in the bulk medium) with the self-focusing Kerr nonlinearity; in this case, the double-channel potential corresponds to two waveguiding slabs embedded in the 3D medium. An alternative optical interpretation is valid in the temporal domain, where Eq. (1) describes the light propagation in a nonlinear planar waveguide with a pair of embedded guiding channels. In the latter case, x is the transverse coordinate, while y is actually the reduced time $t - z/\bar{V}$ (t is physical time, and $\bar{V}$ is the mean group velocity of the carrier wave), assuming that the group-velocity dispersion in the planar waveguide is anomalous.

According to the above interpretations, possible localized solutions of Eq. (1), if it is considered as the GPE, will be interpreted as matter-wave solitons. If the equation is realized as the NLSE in optical media, the localized solutions will be either spatial or spatiotemporal solitons (in the bulk and planar waveguide, respectively; a review of the topic of multidimensional optical solitons can be found in Ref. [22]).

We are looking for stationary solutions as $\Psi(x,y,t) = e^{-i\mu t}\Phi(x,y)$, where real function $\Phi(x,y)$ satisfies equation

$$\mu\Phi + \frac{1}{2}(\Phi_{xx} + \Phi_{yy}) - U(x)\Phi + \Phi^3 = 0, \qquad (3)$$

which can be derived from the Lagrangian

$$L_{\text{stat}} = \frac{1}{2} \int \int dx dy \left[\mu\Phi^2 - \frac{1}{2}(\Phi_x^2 + \Phi_y^2) - U(x)\Phi^2 + \frac{1}{2}\Phi^4 \right]. \qquad (4)$$

Our VA will be based on this Lagrangian.

III. VARIATIONAL APPROXIMATION

A. Symmetry breaking of the two-dimensional solitons

To apply the VA (a detailed account of the technique can be found in Ref. [23]), we assume a situation with two very narrow and deep channels, separated by a broad barrier, i.e., $D \ll L$ in Eq. (2). The corresponding ansatz describing the soliton field configuration consists of two parts. First, inside each channel, i.e., in regions $|x \mp (L+D)/2| < D/2$, we adopt the trial function

$$\Phi(x,y) = A_\pm \cos\left(\pi\frac{x \mp (L+D)/2}{D} \right)\exp\left(-\frac{y^2}{2W^2}\right), \qquad (5)$$

where $A_\pm$ and W are three real variational parameters. In this expression, we assume that the wave function has different amplitudes but equal longitudinal widths W in both channels. In direction x, ansatz (5) emulates the ground state of a quantum-mechanical particle in an infinitely deep potential box, therefore it vanishes at edges of the channel. In direction y, the ansatz is assumed to be a self-trapped soliton, approximated by the Gaussian. The form of the ansatz outside the channels is also suggested by quantum mechanics, emulating a superposition of exponentially decaying ground-state wave functions behind the edges of deep potential boxes

$$\Phi(x,y) = \sum_{+,-} A_\pm \exp\left(-\sqrt{-2\mu}\left|x \mp \frac{L+D}{2}\right| - \frac{y^2}{2W^2}\right), \qquad (6)$$

where amplitudes $A_\pm$ and width W are the same as in Eq. (5).

The substitution of the inner and outer parts of the ansatz, Eqs. (5) and (6), into Lagrangian (4), and subsequent integration over x and y lead to the following effective Lagrangian:

$$\frac{2}{D\sqrt{\pi}}L_{\text{eff}} = \sum_{+,-} \left(\frac{\mu + U_0}{2}A_\pm^2 W - \frac{A_\pm^2}{8W} + \frac{3}{16\sqrt{2}}A_\pm^4 W \right) + \frac{4\sqrt{-2\mu}}{D}e^{-\sqrt{-2\mu}(L+D)}A_+A_-W. \qquad (7)$$

Here, we have adopted the Thomas-Fermi approximation in the x direction (but not along y), by omitting the corresponding kinetic-energy term $-(1/2)\Phi_x^2$ in the Lagrangian density.

Note that ansatz (5) includes the cosine trial function with a constant width. This assumption is relevant for a deeply bound quantum state (as mentioned above, the ansatz was modeled on the pattern of the ground state in the infinitely deep box), but not when the energy eigenvalue $|\mu|$ is small. Indeed, if one tries to predict, by means of this ansatz, a bound state of a particle in a finite-depth rectangular potential well in ordinary (linear) quantum mechanics, one would arrive at a conclusion that the bound state appears only start-

ing from a minimum finite value of U_0, which is, as a matter of fact, the kinetic energy in the x direction. A commonly known exact result is that there is no threshold for the existence of a bound state in any symmetric potential well, even if it is arbitrarily shallow. However, this unphysical effect disappears in the Thomas-Fermi approximation, which was adopted above.

To simplify the notation, we introduce new parameters

$$\epsilon \equiv \mu + U_0 \qquad (8)$$

(notice that ϵ may be both positive and negative),

$$\lambda \equiv (2/D)\sqrt{-2\mu} \exp[-\sqrt{-2\mu}(L+D)], \qquad (9)$$

and $N_\pm \equiv (3/4\sqrt{2})A_\pm^2 W$. Additionally, we define

$$N \equiv \frac{N_+ + N_-}{4\sqrt{\lambda}}, \qquad \nu \equiv \frac{N_+ - N_-}{4\sqrt{\lambda}}. \qquad (10)$$

Norms of the wave function (which are proportional to the numbers of trapped atoms) in the two channels are, according to ansatz (5),

$$\left| \int_{-\infty}^{+\infty} dy \int_{\pm L/2}^{\pm(D+L/2)} dx[\Phi(x,y)]^2 \right| = (\sqrt{\pi}/2)A_\pm^2 DW,$$

hence parameters $N_\pm$ are proportional to the populations in the channels, while ν determines the population imbalance. In terms of this notation, effective Lagrangian (7) transforms into

$$\frac{3}{8\sqrt{2\pi\lambda}D}L_{\text{eff}} = \frac{1}{4\sqrt{\lambda}}\sum_{+,-}\left(\frac{\epsilon N_\pm}{2} - \frac{N_\pm}{8W^2} + \frac{N_\pm^2}{4W}\right) + \frac{\sqrt{\lambda N_+ N_-}}{2}$$

$$\equiv \frac{\epsilon N}{2} - \frac{N}{8W^2} + \frac{\sqrt{\lambda}}{2}\frac{N^2 + \nu^2}{W} + \lambda\sqrt{N^2 - \nu^2}. \qquad (11)$$

This Lagrangian gives rise to variational equations $\partial L/\partial W = \partial L/\partial N = \partial L/\partial \nu = 0$, i.e., respectively,

$$\frac{N}{2\sqrt{\lambda}(N^2 + \nu^2)} = W, \qquad (12)$$

$$\frac{1}{2}\epsilon - \frac{1}{8W^2} + \frac{\sqrt{\lambda}N}{W} + \frac{\lambda N}{\sqrt{N^2 - \nu^2}} = 0, \qquad (13)$$

$$\nu\left(\frac{\sqrt{\lambda}}{W} - \frac{\lambda}{\sqrt{N^2 - \nu^2}}\right) = 0. \qquad (14)$$

Equation (14) has two solutions: $\nu=0$, which, according to Eq. (10) corresponds to symmetric solitons, and asymmetric ones, with $\nu \neq 0$.

In Eqs. (12)–(14), it is relevant to consider N (which is proportional to the total number of atoms) as a given parameter, and ϵ [which is, as the matter of fact, the chemical potential, see Eq. (8)] as an unknown. In this manner, for each value of N we can find the corresponding vales of λ, ϵ,
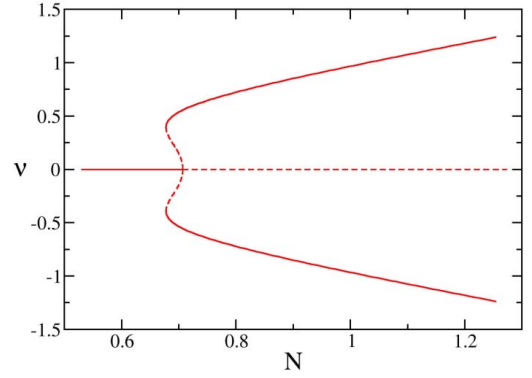

FIG. 2. (Color online) The subcritical symmetry-breaking bifurcation in the double-channel model, as predicted by the variational approximation through Eq. (15). Unstable branches of the solutions are shown by dashed curves.

ν, and W [system (12)–(14) contains only three equations but, as seen from definitions (8) and (9), ϵ and λ are not independent].

Being interested in asymmetric solutions, with $\nu \neq 0$, and substituting expression (12) for W in Eq. (14), we arrive at an equation which determines the population imbalance ν as a function of N:

$$2\sqrt{N^2 - \nu^2}(N^2 + \nu^2) = N. \qquad (15)$$

Notice that this cubic equation for ν^2 does not contain λ, W, or ϵ. The most essential issue is when the SSB occurs, i.e., at what value of N a nontrivial solution for ν appears in Eq. (15).

Straightforward analysis of Eq. (15) demonstrates that, with the increase of N, a pair of physical (real) solutions for ν appears through a tangent (alias saddle-node) bifurcation at $N=N_{\text{min}}=(1/2)\sqrt{3\sqrt{3/2}} \approx 0.677$. At a slightly larger critical value $N_{\text{max}}=1/\sqrt{2}$, a subcritical pitchfork bifurcation takes place, giving rise to solutions splitting off from $\nu=0$. The entire bifurcation diagram for Eq. (15) is displayed in Fig. 2. According to general principles of the bifurcation theory [24], the picture implies that the symmetric solution $\nu=0$ is stable in interval $0 < N < N_{\text{max}}$, and unstable for $N > N_{\text{max}}$. Simultaneously, branches of the asymmetric solutions (those with $\nu \neq 0$) are unstable as long as they go backward, and become stable after they turn forward at point $N=N_{\text{min}}$.

This subcritical bifurcation is qualitatively similar to that explored earlier the model of dual-core nonlinear optical fibers, which is based on a pair of linearly coupled one-dimensional NLSEs for amplitudes of the electromagnetic waves in the two cores [23,25]. On the other hand, in an apparently more complex model of parallel-coupled fiber Bragg gratings, that amounts to a system of four equations with linear and nonlinear couplings, the SSB is simpler, being supercritical (the emerging branches of asymmetric solutions immediately go forward and are stable everywhere) [26].

B. Comparison with the one-dimensional (continuous-wave) case

It is relevant to compare the above results for the SSB of solitons in the 2D model to what can be predicted in the 1D
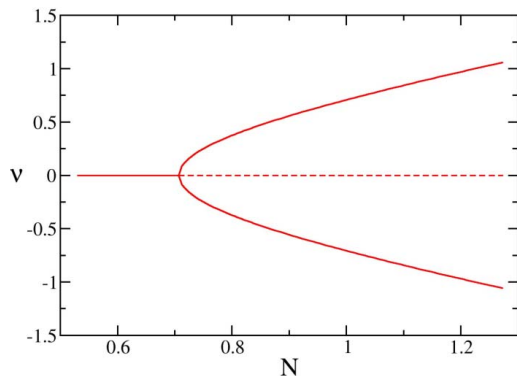
FIG. 3. (Color online) The supercritical symmetry-breaking bifurcation for the cw states, in the 1D model.

counterpart of the model by the same type of the VA. The latter corresponds to the ansatz based on Eqs. (5) and (6), but with $W=\infty$ (in other words, this is a cw state in terms of the 2D model). Then, Lagrangian (7) reduces to

$$L_{\mathrm{eff}} = \mathrm{const} \times \sum_{+,-} \left(\frac{1}{2}\epsilon A_\pm^2 + \frac{3}{16\sqrt{2}}A_\pm^4 + 2\lambda A_+ A_- \right). \quad (16)$$

Straightforward manipulations with the variational equations generated by this Lagrangian, $\partial L_{\mathrm{eff}}/\partial A_+ = \partial L_{\mathrm{eff}}/\partial A_- = 0$, yield a final relation for asymmetric states

$$(A_+^2 - A_-^2)^2 = (A_+^2 + A_-^2)^2 - 2(16\lambda/3)^2. \quad (17)$$

In this context, $N \equiv (3/32\lambda)(A_+^2 + A_-^2)$ is again proportional to the norm, and $\nu \equiv (3/32\lambda)(A_+^2 - A_-^2)$ may be considered as a measure of the asymmetry. The purport of Eq. (17) is that it predicts a critical value of N at which the asymmetric solutions emerge, $N_{\mathrm{cr}} = 1/\sqrt{2}$. As shown in Fig. 3, a principal difference of the SSB for the cw states from its counterpart for the solitons (see Fig. 2) is that the present bifurcation is a supercritical one.

It is relevant to mention that the SSB for the cw solutions of the dual-core-fiber model is also supercritical [27], on the contrary to the subcritical bifurcation for solitons in the same model [25] (the bifurcation of the cw solutions may become subcritical if the nonlinearity is saturable, rather than cubic [27]). Finally, it is also necessary to mention that all the cw states, considered as quasi-1D solutions of the 2D model with the self-attracting nonlinearity, are unstable against modulational perturbations (while solitons may be completely stable in long simulations, see below).

IV. NUMERICAL RESULTS

To verify the above predictions, we solved Eq. (3) numerically, using the imaginary-time relaxation method with a fourth-order Runge-Kutta algorithm. The accuracy of the numerical code was tested by varying computational parameters, namely the mesh density, domain size, and time step. These parameters were then fixed at values for which further increase of the accuracy would not lead to a visible change in the final results [28]. This procedure was applied every time when the physical parameters L, D, N were varied.
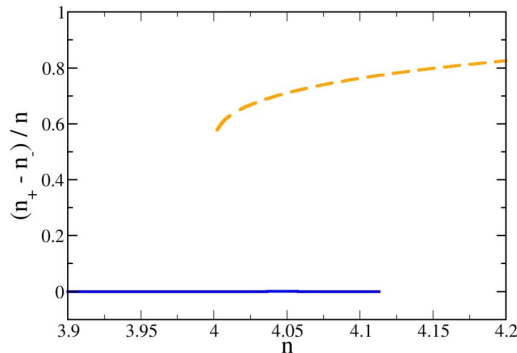

FIG. 4. (Color online) Imbalance in the norm between half-planes $x>0$ and $x<0$, defined as per Eq. (18) for numerically found stationary soliton solutions, versus the total norm. The continuous and dashed lines show, respectively, numerically found stable symmetric and asymmetric solutions (unstable solutions were not generated by the numerical procedure). The parameters are $L=1$, $D=1$, and $U_0=1$.

The stability of solitons produced by this method was then tested by direct integrations of perturbed states in real time. The perturbation was introduced, multiplying the wave function by a symmetry-breaking factor $\Psi \to \Psi(1+\alpha x/L)$. Perturbations with $\alpha=0.05$, which are actually large, were not able to destroy solitons that were identified as stable ones. On the contrary, much small perturbations (for instance, with $\alpha=0.002$) were sufficient to demonstrate instability of those solutions which are unstable, after propagation time $t=100$.

In this work, we did not attempt to identify stability regions for the solitons by computing their eigenvalues in terms of linearized equations for small perturbations, so, in this sense, the stability borders are not completely rigorous ones. Nevertheless, the distinction between unstable and stable solitons revealed by the simulations is very clear, and, on the other hand, the identification of the stability by dint of direct simulations corresponds to experimental conditions, where solitons are subject to various perturbations of a finite size.

The numerical results are summarized in Figs. 4–7. Figure 4 displays a typical dependence of the global asymmetry coefficient for the numerically found soliton solutions, defined as

$$\frac{n_+ - n_-}{n} \equiv \frac{\int_{-\infty}^{+\infty} dy \left[\int_0^{+\infty} \Phi^2 dx - \int_{-\infty}^0 \Phi^2 dx \right]}{\int_{-\infty}^{+\infty} \Phi^2 dx dy}, \quad (18)$$

on the total norm n. The way the figure was generated (through direct simulations converging to stationary states) made is possible to display only stable branches of the solutions, both symmetric and asymmetric ones. Although the unstable branches are missing, there is little doubt that the full SSB diagram corresponding to Fig. 4 is of the generic subcritical type. In particular, a bistability (hysteretic) region, where symmetric and asymmetric solitons coexist and are
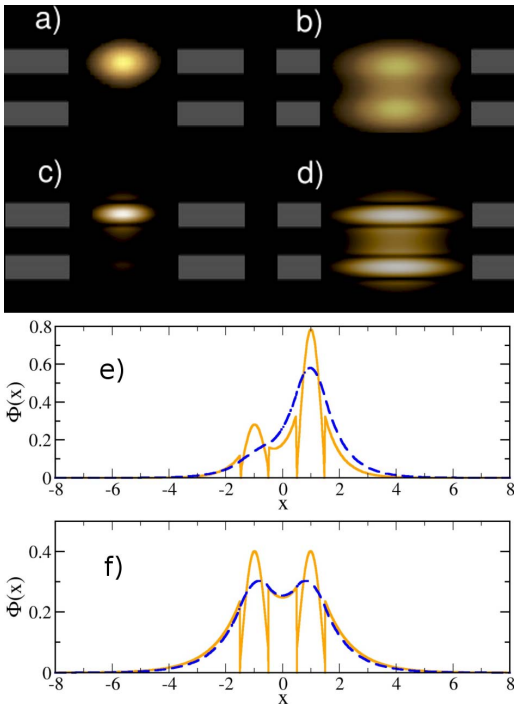
FIG. 5. (Color online) Examples of numerically found asymmetric (a) and symmetric (b) soliton solutions of Eq. (3), for $n=4.05$. Other parameters are the same as in Fig. 4. The gray shading indicates the position of the two potential wells. Panels (c) and (d) show the corresponding solutions as predicted by the variational approximation. In panels (e) and (f), the cross sections of the solutions along $y=0$ are compared: The dashed and solid curves correspond to the numerical and variational solutions, respectively.

simultaneously stable, is obvious in the figure. Thus, the picture suggested by the numerical results is fully consistent with the predictions of the VA shown in Fig. 2.

An example of coexisting symmetric and asymmetric solitons is shown in Fig. 5, for the value of the norm n $=4.05$. While both solitons contain equal total numbers of atoms, the asymmetric one has smaller width in both x and y directions, as its shape provides for stronger effective self-attraction. On the the other hand, the shape of the symmetric soliton features a fair amount of tunneling between the channels. Figures 5(a) and 5(b) were generated by direct numerical simulations, and Figs. 5(c) and 5(d) were obtained from
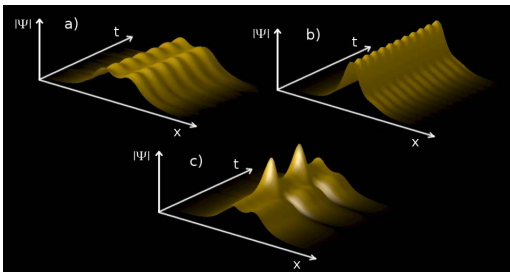

FIG. 6. (Color online) Typical examples of the evolution of perturbed stationary states produced by numerical simulations of Eq. (1). (a) A stable symmetric state for $n=3.9$. (b), (c) Stable asymmetric and unstable symmetric states for $n=4.15$. Other parameters are as in Fig. 4. The evolution time is $t=300$.
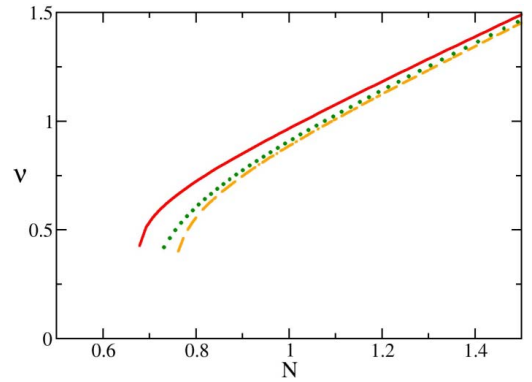

FIG. 7. (Color online) Comparison of the variational prediction for the asymmetric solitons (solid line) with numerical results (dotted and dashed lines). The dashed curve corresponds to the same parameters as in Fig. 4, while the dotted one is generated by the numerical solution of Eq. (3) with the distance between the wells increased to $L=2$.

the VA. It is observed that the agreement between the numerical and variational results is quite good. For a more detailed comparison, we display cross-sections of both solitons in panels (e) and (f).

Figure 6 illustrates the stability of various solitons in numerical simulations. Below the bifurcation point (for $n=3.9$), we present stable evolution of the symmetric state, and above the bifurcation we demonstrate a stable asymmetric state for $n=4.15$. Also, for norm $n=4.15$, we display the evolution of the unstable symmetric state. It is worthy to note that this unstable state does not simply relax to the stable one, but rather performs persistent oscillations between symmetric and asymmetric shapes.

In Fig. 7, we present comparison of the analytical results, obtained by means of the VA for the family of asymmetric solitons, with numerical findings. The solid line is the $\nu(N)$ dependence corresponding to the stable upper branch of the plot in Fig. 2, whereas the other two lines show two sets of the corresponding numerical results, generated as noted in the caption to Fig. 7. Generally, the solid line (variational solution) is shifted towards smaller values of N.

V. CONCLUSIONS

In this work, we have introduced a physical model that gives rise to the SSB of 2D solitons in a dual-core system; previously, this effect was studied in detail, but solely in 1D settings. Our model is based on the 2D nonlinear Schrödinger equation with the self-focusing cubic nonlinearity and a quasi-1D double-channel potential. The model applies to the description of spatial optical solitons in a bulk medium with two waveguiding slabs embedded into it, or spatiotemporal solitons in a planar waveguide into which two guiding channels were inserted. The same model may also be interpreted as the Gross-Pitaevskii equation for a pancake-shaped Bose-Einstein condensate trapped around two attractive parallel light sheets. By means of the VA, we have predicted the SSB bifurcation for the 2D solitons supported by the double channel. The bifurcation was predicted

to be subcritical (unlike its counterpart in the continuous-wave 1D model). The predictions of the VA are well corroborated by numerical solutions.

ACKNOWLEDGMENTS

[1] S. Burger, K. Bongs, S. Dettmer, W. Ertmer, K. Sengstock, A. Sanpera, G. V. Shlyapnikov, and M. Lewenstein, Phys. Rev. Lett. **83**, 5198 (1999); J. Denschlag, J. E. Simsarian, D. L. Feder, C. W. Clark, L. A. Collins, J. Cubizolles, L. Deng, E. W. Hagley, K. Helmerson, W. P. Reinhardt, S. L. Rolston, B. I. Schneider, and W. D. Phillips, Science **287**, 97 (2000).

[2] L. Khaykovich, F. Scherck, G. Ferrari, T. Bourdel, J. Cubizolles, L. D. Carr, Y. Castin, and C. Salomon, Science **296**, 1290 (2002); K. E. Strecker, G. B. Partridge, A. G. Truscott, and R. G. Hulet, Nature (London) **417**, 153 (2002); S. L. Cornish, S. T. Thompson, and C. E. Wieman, Phys. Rev. Lett. **96**, 170401 (2006).

[3] B. Eiermann, Th. Anker, M. Albiez, M. Taglieber, P. Treutlein, K.-P. Marzlin, and M. K. Oberthaler, Phys. Rev. Lett. **92**, 230401 (2004).

[4] B. D. Josephson, Phys. Lett. **1**, 251 (1962).

[5] K. K. Likharev, Rev. Mod. Phys. **51**, 101 (1979).

[6] S. V. Pereverzev, A. Loshak, S. Backhaus, J. C. Davis, and R. E. Packard, Nature (London) **388**, 449 (1997).

[7] K. Sukhatme, Y. Mukharsky, T. Chui, and D. Pearson, Nature (London) **411**, 280 (2001).

[8] M. Albiez, R. Gati, J. Fölling, S. Hunsmann, M. Cristiani, and M. K. Oberthaler, Phys. Rev. Lett. **95**, 010402 (2005); see also a review, R. Gati and M. K. Oberthaler, J. Phys. B **40**, R61 (2007).

[9] J. Javanainen, Phys. Rev. Lett. **57**, 3164 (1986).

[10] M. W. Jack, M. J. Collett, and D. F. Walls, Phys. Rev. A **54**, R4625 (1996).

[11] I. Zapata, F. Sols, and A. J. Leggett, Phys. Rev. A **57**, R28 (1998).

[12] G. J. Milburn, J. Corney, E. M. Wright, and D. F. Walls, Phys. Rev. A **55**, 4318 (1997).

[13] A. Smerzi, S. Fantoni, S. Giovanazzi, and S. R. Shenoy, Phys. Rev. Lett. **79**, 4950 (1997).

[14] S. Raghavan, A. Smerzi, S. Fantoni, and S. R. Shenoy, Phys. Rev. A **59**, 620 (1999).

[15] F. S. Cataliotti, S. Burger, C. Fort, P. Maddaloni, F. Minardi, A. Trombettoni, A. Smerzi, and M. Inguscio, Science **293**, 843 (2001).

[16] F. S. Cataliotti, L. Fallani, F. Ferlaino, C. Fort, P. Maddaloni, and M. Inguscio, New J. Phys. **5**, 71 (2003).

[17] T. Anker, M. Albiez, R. Gati, S. Hunsmann, B. Eiermann, A. Trombettoni, and M. K. Oberthaler, Phys. Rev. Lett. **94**, 020403 (2005).

[18] S. Raghavan, A. Smerzi, S. Fantoni, and S. R. Shenoy, Phys. Rev. A **59**, 620 (1999).

[19] K. W. Mahmud, H. Perry, and W. P. Reinhardt, Phys. Rev. A **71**, 023615 (2005).

[20] E. Infeld, P. Zin, J. Gocalek, and M. Trippenbach, Phys. Rev. E **74**, 026610 (2006).

[21] L. D. Carr, Charles W. Clark, and W. P. Reinhardt, Phys. Rev. A **62**, 063610 (2005); **62**, 063611 (2000).

[22] B. A. Malomed, D. Mihalache, F. Wise, and L. Torner, J. Opt. B: Quantum Semiclassical Opt. **7**, R53 (2005).

[23] B. A. Malomed, in *Progress in Optics*, edited by E. Wolf (North Holland, Amsterdam, 2002), Vol. 43, p. 71.

[24] G. Iooss and D. D. Joseph, *Elementary Stability and Bifurcation Theory* (Springer-Verlag, New York, 1980).

[25] B. A. Malomed, I. M. Skinner, P. L. Chu, and G. D. Peng, Phys. Rev. E **53**, 4084 (1996).

[26] W. Mak, B. A. Malomed, and P. L. Chu, J. Opt. Soc. Am. B **15**, 1685 (1998).

[27] A. W. Snyder, D. J. Mitchell, L. Poladian, D. R. Rowland, and Y. Chen, J. Opt. Soc. Am. B **8**, 2102 (1991).

[28] Most of the numerical simulations were performed using the following set of parameters: time step $\Delta t = 0.01$, mesh density $\Delta x = \Delta y = 0.1$, and domain size $x_{max} = y_{max} = 8$.